Acta Materialia 241 (2022) 118384

Contents lists available at ScienceDirect

Acta Materialia

journal homepage: www.elsevier.com/locate/actamat

Full length article

Anomalous kinetics, patterns formation in recalescence, and final microstructure of rapidly solidified Al-rich Al-Ni alloys

P.K. Galenko[a,b,*], L.V. Toropova[c], D.V. Alexandrov[b], G. Phanikumar[e], H. Assadi[f], M. Reinartz[a,d], P. Paul[a], Y. Fang[a], S. Lippmann[a]

[a] Otto-Schott-Institut für Materialforschung, Friedrich-Schiller-Universität-Jena, Jena 07743, Germany
[b] Laboratory of Multi-Scale Mathematical Modeling, Department of Theoretical and Mathematical Physics, Ural Federal University, Lenin Ave., 51, Ekaterinburg, 620000, Russian Federation
[c] Laboratory of Mathematical Modeling of Physical and Chemical Processes in Multiphase Media, Department of Theoretical and Mathematical Physics, Ural Federal University, Lenin Ave., 51, Ekaterinburg, 620000, Russian Federation
[d] Institut für Materialphysik im Weltraum, Deutsches Zentrum für Luft- und Raumfahrt (DLR-Köln), Linder Höhe, 51147 Köln, Germany
[e] Department of Metallurgical and Materials Engineering, Indian Institute of Technolgy Madras, Chennai 600036 India
[f] Brunel University London, BCAST, Uxbridge, Middlesex UB8 3PH, United Kingdom

ARTICLE INFO

Article history:
Received 24 July 2022
Revised 19 September 2022
Accepted 23 September 2022
Available online 29 September 2022

Keywords:
Rapid solidification
Microgravity
Nucleation and growth
Dendritic microstructure

ABSTRACT

From thermodynamical consideration, rather a monotonically increasing crystal growth velocity with increasing undercooling is expected in the crystallization of liquids, mixtures, and alloys [P.K. Galenko and D. Jou, Physics Reports 818 (2019) 1]. By contrast to this general theoretical statement, Al-rich Al-Ni alloys show an anomalous solidification behavior: the solid-liquid interface velocity slows down as the undercooling increases [R. Lengsdorf, D. Holland-Moritz, D. M. Herlach, Scripta Materialia 62 (2010) 365]. It is also found that besides the anomalous growth behaviour, changes in the shape of the recalescence front as the growth front morphology occur. In the light of recent measurements in microgravity with an Al-25at.% Ni alloy sample onboard the International Space Station (ISS) results confirming this anomalous behavior as an unexpected trend in solidification kinetics are presented. The measurements show multiple nucleation events forming the growth front, a mechanism that has been observed for the first time in Al-Ni alloys [D. Herlach et al., Physical Review Materials 3 (2019) 073402; M. Reinartz et al. JOM 74 (2022) 2420] and summarized with detailed analysis in the present publication over a wider range of concentrations. Particularly, the experimental measurements and obtained data directly demonstrate that the growth front does thus not consist of dendrite tips (as in usual rapid solidifying samples), but of newly forming nuclei propagating along the sample surface in a coordinated manner. Theoretical analysis on intensive nucleation ahead of crystal growth front is made using the previously developed model [D.V. Alexandrov, Journal of Physics A: Mathematical and Theoretical 50 (2017) 345101]. Using equations of this model, quantitative calculations confirm the interpretation of experimentally observed propagation of the recalescence front and obtained data on the microstructure of droplets solidified in electromagnetic levitation facility (EML) on the Ground, under reduced gravity during parabolic flights, and in microgravity conditions onboard the ISS.

1. Introduction

The developed methods of containerless processing of elemental or alloying samples allow us to reach deep undercooling or high-temperature gradients in the liquid that initiates rapid solidification of these samples [1]. Rapid solidification provides various pathways to freeze (meta)stable phase leading to special properties for processed materials [2]. A special place in the study of rapidly solidifying alloys is occupied by aluminum-nickel alloys due to their practical significance. In particular, Al-Ni alloys are used as a basis for obtaining magnetically hard materials with high values of coercive force and residual induction (Fe-Ni-Al alloys). Also, Al-Ni alloys are a basic system for high-temperature alloys exhibiting improved mechanical properties. Therefore, Al-Ni alloys were intensively investigated especially by rapid solidification techniques in different directions simultaneously.

* Corresponding author.
E-mail address: peter.galenko@uni-jena.de (P.K. Galenko).

https://doi.org/10.1016/j.actamat.2022.118384

First, Assadi et al. [3–5] performed basic initial experiments with the EML focusing on the Ni-rich side of the Al-Ni system. In particular, using this developed EML-method for quantitative estimation of crystal growth velocity by propagating fronts of recalescence, effect of forced flow on the dendritic microstructure was studied [6–8]. The experiments were performed both by containerless electromagnetic levitation (EML) on Earth and under reduced gravity conditions during parabolic flight campaigns. The alternating electromagnetic fields induce convection, which is strong under terrestrial conditions while much weaker in reduced gravity. By comparing results obtained on Earth and in reduced gravity, it was demonstrated that the change of transport conditions by convection significantly alters the kinetics of solidification and the evolution of grain refined microstructures at undercoolings less than 100 K [9].

Second, Al-Ni alloys are typical multi-phase alloys that easily may exhibit different phases for the same chemical composition but depend on the degree of undercooling. Applying X-ray diffraction analysis, identification of phases during solidification of samples *in-situ* as well as during the post-recalescence period of the solid samples at their cooling *post-mortem* was provided by Shuleshova et al. [10–13]. Particularly, a search for disordered phases was carried out in which the main attention in the study was paid to the transition from an ordered to a disordered phase of an intermetallic compound of the $Ni_{50}Al_{50}$ composition [14]. This transition has been intensively studied at the atomic level by molecular dynamics simulation [15,16], and at the mesoscopic spatial level using the phase field method [17,18]. *In situ* diffraction of synchrotron radiation on levitation-processed samples of the $Ni_{50}Al_{50}$ alloy unambiguously shows a transition from ordered to disordered growth at the critical undercooling $\Delta T^* \approx$ 250K [19]. The complete transition at this critical value of undercooling is accompanied by a steep rise of the crystal growth velocity of a congruently melting intermetallic phase. This sharp transition in crystal growth kinetics is attributed to disorder trapping during the non-equilibrium solidification of deeply undercooled melts [20] consistently to the theory of kinetic phase transitions [21–26].

Third, the remarkable feature of Al-Ni alloys is their absolutely unusual solidification kinetics in the wide concentration range of the Al-rich part of the phase diagram, namely in samples of Al-25...40 at.% Ni alloys. Indeed, with increasing undercooling, the difference in Gibbs free energy between the liquid and the primary solid phase increases, and the growth velocity of the solid phase depends directly on the difference in the Gibbs free energies [27]. It is hence expected that the growth velocity increases with increasing undercooling. Lengsdorf et al. [28,29] used the EML technique [1,2] to investigate the growth velocity *versus* undercooling relationship in Al-Ni alloys. They found that, as opposed to the expected trend, the growth velocity decreases for increasing undercooling in Al-rich Al-Ni alloys at least in a certain temperature range. This finding contradicts common theory of crystal growth, according to which only increasing growth velocities are dynamically stable [30,31].

We shall pay mainly our attention to the above principally important *Third* issue with the main goals of the present work as

(*a*) to compare the new experimental results obtained for samples of Al-Ni alloys under microgravity conditions onboard the ISS with the results obtained previously for samples processed in EML under terrestrial conditions [29],

(*b*) following the terminology and systematization given in the work [32], to classify and unify the structures experimentally obtained in the process of recalescence and in the final crystalline microstructure of samples solidified onboard the ISS,

(*c*) following a qualitative explanation of the anomalous kinetics of solidification of Al-Ni alloys [33], to give a quantitative assessment and confirmation of the discussed mechanism of anomalous solidification based on the solution of model equations [34,35].

The fulfillment of these (*a*)-(*c*)-goals will make it possible to complete the explanation of the mechanism of anomalous solidification of Al-rich Al-Ni alloys, which was begun in the pioneering works [28,29].

2. Experimental

In order to study the relationship between the dendrite growth velocity, undercooling, and microstructure, electromagnetic levitation experiments were carried out using four different Al-Ni compositions, particularly Al-25at.% Ni, Al-31.5at.% Ni, Al-40at.% Ni and Al-45at.% Ni, see Fig. 1. Samples were prepared from Al 5N (Hydro Aluminium Rolled Products GmbH, Bonn, Germany), and Ni $4N_5$ (AlfaAesar Puratronic). The materials were alloyed using an induction furnace with a cold wall crucible under Ar atmosphere. Levitation samples were cut from the as-cast button by using a precision saw (IsoMet5000, Buehler). The alloys Al-31.5at.% Ni, Al-40at.% Ni and Al-45at.% Ni were solely studied under 1*g* conditions, whereas the alloy Al-25at.% Ni was additionally studied onboard the ISS under microgravity. 1*g* conditions require a strong levitation force which, in fact, induces the forced convective flow inside the bulk of the molten droplet. As such, because the melt velocity is directly influenced by the applied electromagnetic field strength, microgravity experiments have the advantage due to the actually negligible fluid flow in molten droplets under lower electromagnetic field strength, decoupled heating, and positioning [2].

In the experiments, undercoolings of up to $\Delta T \approx$ 260K under 1*g* and up to $\Delta T \approx$ 350K under microgravity were reached. A high-speed camera (Phantom v7.3, Amatek Vision Research) was used to record the growth front with frame 80 rates of up to 20 000 frames per second (fps). An infrared pyrometer (IDA 140 MB 30L, LumaSense Technologies) was applied to record the temperature-time profiles during the processing on the Ground and onboard the ISS for samples with a diameter of 6.5-7.2 mm.

After processing in the electromagnetic levitator on the Ground, the samples were cut to halves and mounted in electrically conductive embedding material (PolyFast, Struers) for analysis in a scanning electron microscope (LEO 1530 85 VP, Zeiss Merlin). Finally, some other details of the experimental technique as well as typical heating-and-cooling curves "temperature-time" for the droplet processed in EML are described in our recent publication [33].

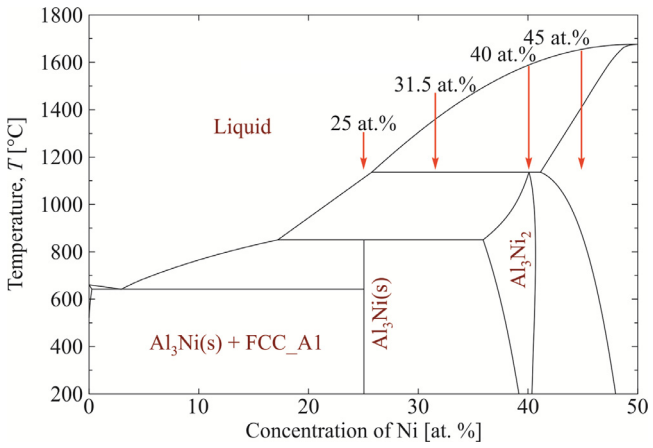

Fig. 1. Section of the phase diagram of Al-Ni with alloy compositions used in the present work: Al-25at.% Ni, Al-31.5at.% Ni, Al-40at.% Ni and Al-45at.% Ni. The phase diagram was calculated using FactSage 7.1 [44] with the SGTE 2014 data base [11,45].

3. Solidification kinetics of Al-Ni-alloys

3.1. Solidification velocity

Previous measurements using Al-rich Al-Ni alloys showed a decreasing solidification velocity for increasing undercooling as an anomalous behaviour of the solidification velocity-undercooling relationship [28,29,32,33]. Such downward tendency is shown by the solid black triangles in Fig. 2 as well as by velocities determined in space under microgravity conditions. Current measurements are shown with differently coloured and shaped markers representing different front morphologies. These results of our novel experiments confirm the growth front velocity measurements by Lengsdorf et al. [28,29].

Note that for Al-25at.% Ni, a maximum in the solidification velocity at around $\Delta T \approx 150$K is visible in Fig. 2(a). This maximum is associated with the appearance of new phase. However, the number of data points for the Al-25at.% Ni alloy gained onboard the ISS (see red circles and green diamonds in Fig. 2(a)) is limited and too small to reproduce the peak observed in the velocity-undercooling relationship for the values of undercoolings of $150 < \Delta T(\mathrm{K}) < 200$. In any case, the overall trend shows a decreasing solidification velocity with increasing undercooling. In the Al-31.5at.% Ni alloy, shown in Fig. 2(b), the velocity decreases monotonically. For compositions above $C_{Al} \approx 35$at.%, the velocity passes through a minimum as the undercooling increases that is demonstrated by Fig. 2(c). For $C_{Al} \geq 45$at.%, the velocity shows the expected trend of a monotonically increasing solidification velocity as the undercooling increases.

The downward parts of the velocity curves shown in Fig. 2(a)-(c) contradict general crystal growth theory according to which only the curves with positive slope $dV/d(\Delta T) > 0$ are dynamically stable [30,31]. Instead, kinetic curves with a negative slope, $dV/d(\Delta T) < 0$, are dynamically unstable, demonstrated by the prediction that growth conditions leading to $dV/d(\Delta T) < 0$ cannot attain a steady state. The growth behavior exhibiting the downward velocity curves present anomaly in growth kinetics of Al-rich Al-Ni alloys (see Fig. 2(a)-(c)).

Different modeling attempts were made to obtain mechanism or merely explain this anomaly.

(*i*) Ehlen and Herlach [46] considered different properties of the involved phases, interpreting the AlNi B2 phase either as a solid solution or an intermetallic phase. Growth velocities in the correct magnitude were achieved, but the negative slope $dV/d(\Delta T) < 0$ of the velocity-undercooling relationship was not reproduced.

(*ii*) Several interesting hypotheses have been put forward to explain the downward branch of the velocity curve with increasing supercooling. For example, hypotheses about the effect on the growth rate of dendrites were associated with the influence of forced convection, inverse melting, varying fractions of the solidifying phases, and non-stationarity of the temperature field inside the droplet. However, the inconsistency of all these hypotheses in connection with the influence on the kinetics of dendritic growth in Al-Ni alloys and the change in the slope of the velocities curves was discussed in detail in Reinartz's dissertation [47].

(*iii*) Mullis [48] supposed that the enhancement of the velocity at the surface and the trend for decreasing velocity with the increase of undercooling occurs due to enrichment of the droplet surface by the nickel. This enrichment probably appears because the sample processes in EML under high purity vacuum may lose Al at the surface due to its evaporation at low undercooling (i.e., at high temperature). Such speculation is based on the possible fact that the oxidation of surface Al, followed by evaporation of the oxide, so that the surface becomes more Ni-rich relative to the bulk. As this may significantly alter the liquidus temperature, the effective undercooling of the thin surface layer becomes higher than that of the bulk which initiate intensive surface crystal nucleation and their growth. By the developing model which takes into account different Ni-content at the surface of droplets and, respectively, different undercooling, Mullis calculated downwards velocity curve for the small and intermediate values of undercooling and upwards curve for the velocity at higher undercooling. Indeed, his calculating predictions showed consistency with experimental data for the Al-35% Ni and Al-40% Ni alloys, see Fig. 14 in [48], especially, exhibiting existence of the kinetic curves with a negative slope, $dV/d(\Delta T) < 0$. In this case of changing chemical content with temperature the theorem about thermodynamically allowed regimes only for kinetic curves with positive slope, $dV/d(\Delta T) > 0$, and without alternating chemical composition [30,31], might not be applied directly. Anyway, the main difficulty of accepting the downwards velocity curves of Mullis is how to combine the kinetic curves for velocity shown in Fig. 14 of his paper [48], which were calculated only for the growth of dendrites, with the experimentally observed recalescence front, which propagates by the predominant nucleation of crystals on the surface of the droplet at small and moderate undercoolings [32,33].

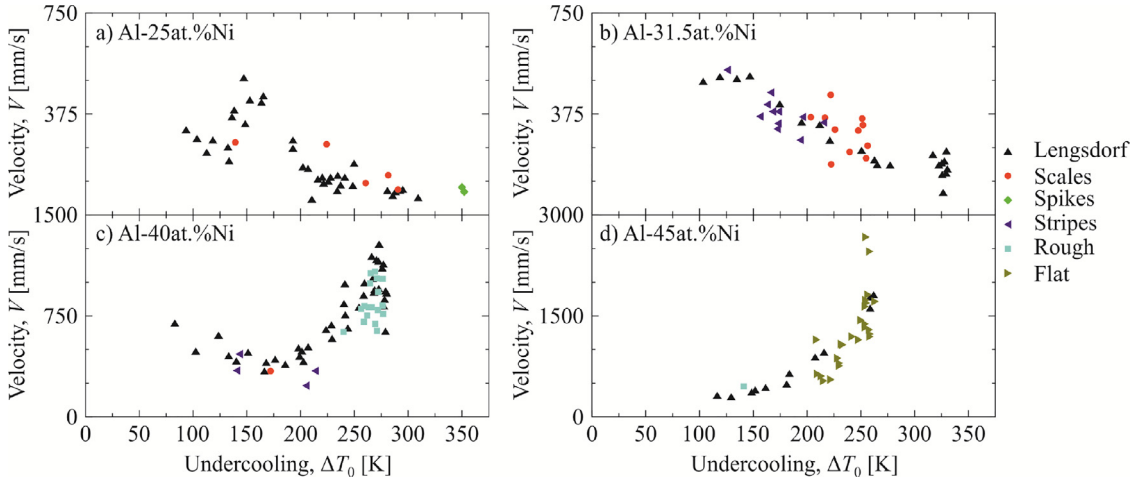

Fig. 2. Measured solidification front velocities for four different compositions: (a) Al-25at.% Ni, (b) Al-31.5at.% Ni, (c) Al-40at.% Ni and (d) Al-45at.% Ni. Microgravity results, filled markers, are available only for the Al-25at.% Ni alloy. Literature values by Lengsdorf et al. [28,29] are marked by black triangles. Five different growth front morphologies are represented by differently coloured and shaped markers.

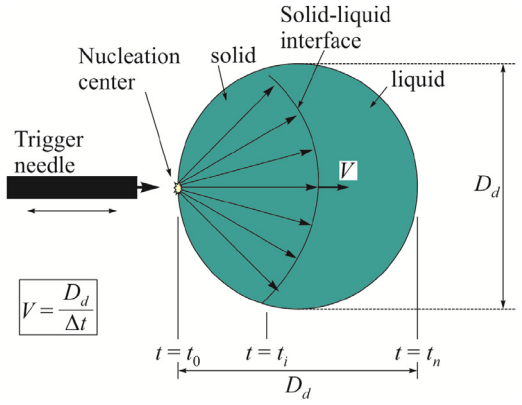

Fig. 3. Scheme for measurement of the solidification front velocity in sample (droplet) processed by EML. Here: d is the diameter of the droplet which is assumed to be spherical and t is the time. The recalescence front with the velocity V is shown at the time t_i. The measurement of the solidification velocity is shown here by the method of "first frame - last frame" [49], i.e. V is measured from the time, t_0 for nucleation of crystals up to the time t_n for the recalescence front to pass through the surface of the entire droplet.

Taking the above (*i*)-(*iii*) points into account we formulate the main idea about negative slopes of the velocity curves in the Al-Ni alloys by the followed analysis of the recalescence fronts, solidification front morphology, metallography of samples, and, especially, by theoretical calculations of the rates for solidification fronts.

3.2. Shape of recalescence fronts and growth morphologies

The high-speed camera captures the videos at frame rates of up to 20 000 fps. The obtained movies allow us to determine the solidification velocity as a velocity for the recalescence front propagation. Recollect that recalescence is the process of releasing (excess) latent heat during the transition from a liquid to a solid crystalline state. The region in which the transition occurs and where latent heat is released is observed as bright and light, and the region where the transition does not yet occur is observed as dark. Therefore, the recalescence front is the interface between the released and not yet released latent heat of crystallization. Usually, the recalescence front coincides with the surface around the tips of growing crystals. Therefore, the solidification velocity is measured by the geometrical envelope propagation of the crystals (dendritic) tips. Figure 3 demonstrates a scheme for the solid-liquid interface velocity measurement by the recalescence front propagating in solidifying droplet. The solidification starts after triggering this process by the needle (which is measured at the same material as the droplet itself) at the initial time t_0. The primary solidification is finished at the time t_n, therefore, the solid-liquid interface velocity is estimated by the ratio $V = D_d/\Delta t$ with D_d the droplet diameter and $\Delta t = t_n - t_0$. Such estimation is known as the measurement by "the first frame - last frame" in comparison with the other method of the velocity measurement known as "frame by frame" [49]. Finally, besides the front velocity, the morphology of the front is determined.

3.2.1. Al-25at.% Ni.

At undercoolings of $\Delta T < 300$K, the nucleation front consists of numerous circular features that we will call "scales" following definition given in the work [32], see Fig. 4(a). The sequence of new scales forming next to the previous ones continues in a stable manner throughout the whole solidification time of the droplets for $\Delta T < 300$K.

Figure 4 (b) shows a second front morphology which may also exist in the solidifying Al-25at.% Ni alloy. For undercoolings of $\Delta T > 300$K, the front shows dendrite like features with sharp tips. Because this has not been observed on Earth so far, the microstructure has not been studied in detail yet, and we designate the morphology of the growth front as spikes.

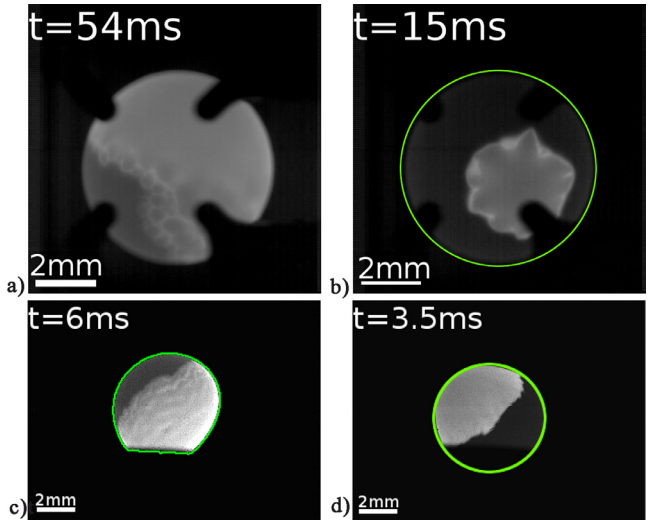

Fig. 4. Growth front morphologies as snapshots of the recalescence fronts at the sample surface were observed and fixed by the high-speed camera. The time (in milliseconds) of the concrete snapshot is indicated at the left-top corner. Magnification is indicated by the scale at the left-bottom corner in every image. The green outline limits the visible area of the levitating droplet, where the propagation of the recalescence front and the crystalline microstructure were analyzed. (a) Solidification front represented by scales in Al- 25at.% Ni solidifying at $\Delta T = 282$K. (b) Solidification front with spikes (dendrites with sharp tips) in Al- 25at.% Ni solidifying at $\Delta T = 350$K. (c) Stripes (wavy fronts) behind the solidification front in Al-31.5at.% Ni solidifying at $\Delta T = 216$K. (d) Rugged (rough) solidification front in Al-40at.% Ni solidifying at $\Delta T = 277$K.

3.2.2. Al-31.5at.% Ni.

For this alloy, two different morphologies were observed: similar to Al-25at.% Ni, scales appear, here for undercoolings above $\Delta T \approx 200$K. At undercoolings below $\Delta T \approx 200$K, a different morphology is found. The solid part of the sample surface exhibits stripes, which are brighter than their surroundings, see 4(c). They are essentially parallel to the solidification front. We call this morphology wavy because it seems like the scales could have merged into stripes. However, in contrast to the morphology in Fig. 4(a), no clearly distinct scales appear close to the growth front. In the range of undercooling, $200 < \Delta T(\text{K}) < 220$, a transition region from wavy to scales was observed, where both morphologies occur. The transition from wavy to scales could not always be clearly identified.

3.2.3. Al-40at.% Ni.

During the solidification of this alloy, the wavy growth front morphology appeared for undercoolings of $\Delta T < 220$K. The morphology occasionally was scale-like, but in other cases, it was similar to the morphologies in Al- 31.5at.% Ni where the scales have probably merged to stripes. For $\Delta T > 220$K, a rugged front was observed. Figure 4(d) shows an example of this rugged morphology.

3.2.4. Al-45at.% Ni.

The morphology in this alloy was observed as similar to the morphology of the Al- 40at.% Ni alloy shown in Fig. 4(d) at $\Delta T > 220$K. For instance, at the undercooling of $\Delta T = 141$K a rugged interface was observed in the Al-45at.% Ni alloy. For higher undercoolings, the front became smoother and the rugged structure only appeared at the end of solidification. In Fig. 5, a flat front is shown, which, in comparison to Fig. 4(d), shows only weak disturbances.

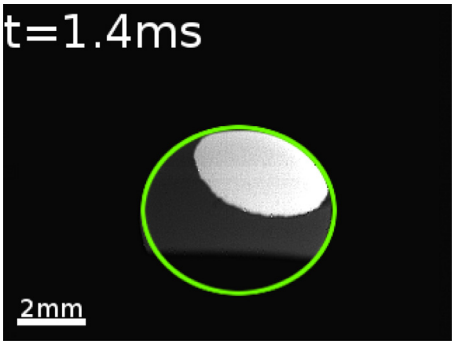

Fig. 5. Flat (planar) growth front in Al- 45at.% Ni solidifying at $\Delta T = 241$K. The time (in milliseconds) of this snapshot is indicated at the left-top corner. Magnification is indicated by the scale at the left-bottom corner of this image.

It is worth noting that the transition to a macroscopically smooth front of recalescence (see Fig. 4(d) and 5), prevails in many recorded movies on high-speed crystallization of droplets in levitators if the undercooling is equal to or exceeds some critical value. Such a transition from a macroscopically angular front (as, for example, is observed in Fig. 4(b)) to a flat front is associated with a change in the crystallization regime. For example, a transition to a macroscopically smooth (flat) front occurs if crystal growth becomes controlled not only by heat removal but occurs in a thermokinetic regime, in which atomic kinetics controls the velocity and morphology of the front together with the heat removal from the interface [50,51].

3.3. Microstructure in Al-25at.% Ni

A thorough microstructure analysis was carried out for the Al-25at.% Ni alloy processed in EML on the Ground. In this alloy, a negative slope of the velocity V-curve was found for the whole range of measured undercoolings ΔT, see Fig. 2(a). Two samples that were processed at the undercooling of $\Delta T = 85$K, see Fig. 6, and at the undercooling $\Delta T = 137$K, see Fig. 7, were prepared for microstructure analysis through the geometrical centre of these samples.

Figure 6 (a) shows an optical image (polarized light) of the microstructure exhibiting the extensive shrinkage holes in the centre of sample (solidified at $\Delta T = 85$K)[1]. Within the entire visible microstructure, the shrinkage pores are completely enclosed by solid. In the solid around the shrinkage holes, dendritic structures are visible. These are marked in Fig. 6(b) with an arrow. At distances of approximately 200 μm, these structures appear on the whole outer surface of the sample.

The microstructure of the second sample (solidified at $\Delta T =$ 137K) is shown in Fig. 7. The dendrites growing towards the sample centre are clearly visible. Most of the dendrites do not exhibit secondary arms. The orientation of the dendrites indicates that nucleation occurs in multiple events at the sample surface, leading to a region of growth selection and growth of the favourably oriented dendrites towards the sample centre.

There are several additional compelling facts about the multiple nucleation as the most promising explanation for the anomalous behavior of the velocity shown in Fig. 2(a)-(c). For example, there are many histograms "nucleation of crystals in time", appearance of "scales in time" [47], but the data given here (see, for instance, Figs. 6 and 7) is very representative to assert that we observe the front of nucleation competing with

[1] To obtain a better contrast in the image, the mounting resin was masked. Therefore, these shrinkage holes are emphasized by masking the reflections from inside the holes by using a bright-field image.

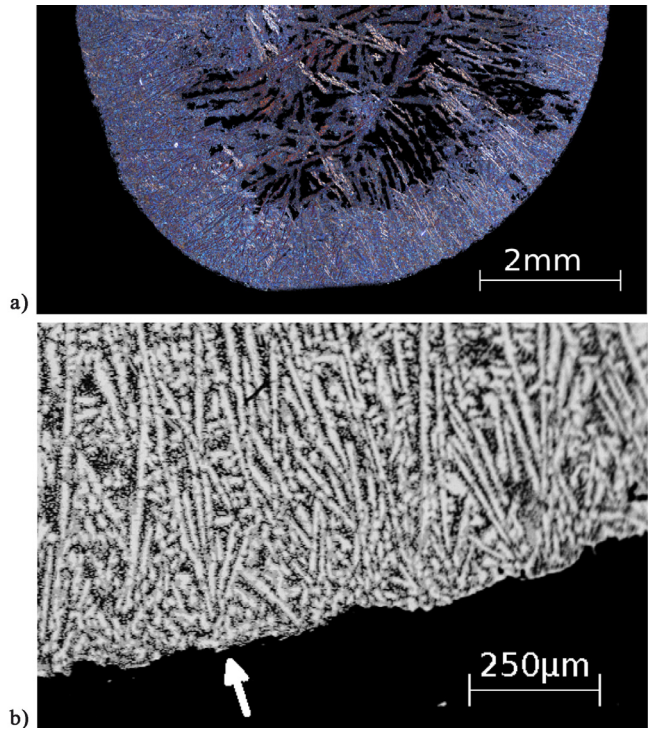

Fig. 6. Microstructure of an Al-25at.% Ni alloy solidified at an undercooling of $\Delta T = 85$K. (a) Microstructure in polarized light. The image shows large shrinkage holes inside the sample. (b) Scanning electron microscope image of the sample edge. The arrow marks an example for dendrites growing from the sample surface in the direction of the sample center.

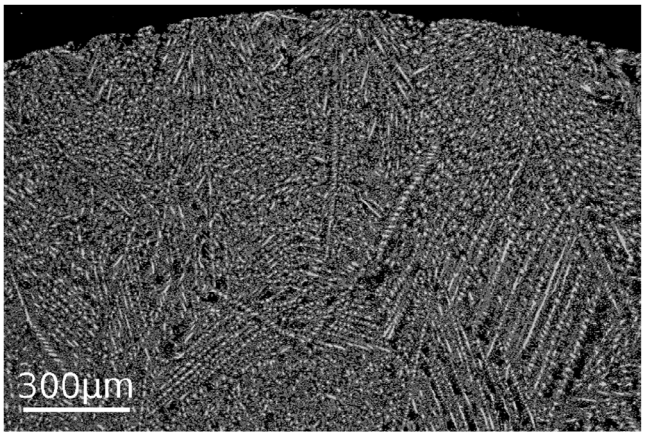

Fig. 7. Scanning electron microscope image of an Al- 25at.% Ni sample solidified at $\Delta T = 137$K. Dendritic structures grown inward from the sample surface are found around the whole sample surface. Bright phase is Al_3Ni, grey phase is α-Al, the rest is represented by pores.

the crystal growth process that might give downward velocity curves ($dV/d(\Delta T) < 0$) for solidifying samples of Al-25...40 at.% Ni alloys.

Figure 8 shows a part of the Al-25at.% Ni droplet solidified at the undercooling $\Delta T = 123$K. Such undercooling is related to the velocity belonging to the downward part of the curve which is shown in Fig. 2(a). Even though the dendrites are visible as growing inward from the outer surface of the droplet to its center, the final structure exhibits a junction of differently oriented grains formed upon multiple crystal nucleation.

Additionally, one can compare the dendritic structure of samples solidified within different ranges of undercooling at which

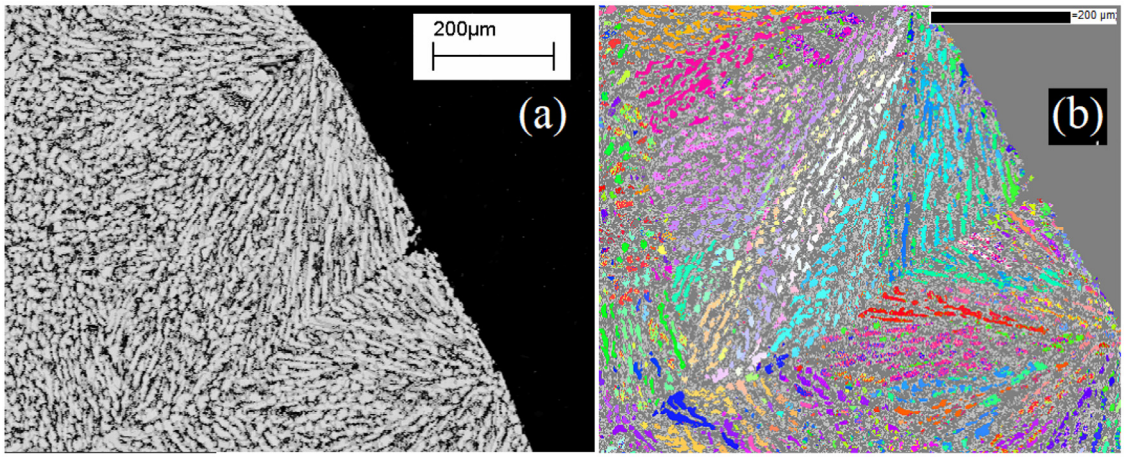

Fig. 8. A part of the Al-25at.% Ni droplet solidified at the undercooling $\Delta T = 123$K which is consistent with the downward part of the velocity curve shown in Fig. 2(a). Primary dendrites consist of the Al_3Ni_2-phase. The droplet was solidified under reduced gravity in EML established onboard ISS. (a) Image obtained by scanning electron microscope (SEM). (b) The same part of the droplet shown after analysis provided by Electron backscatter diffraction (EBSD).

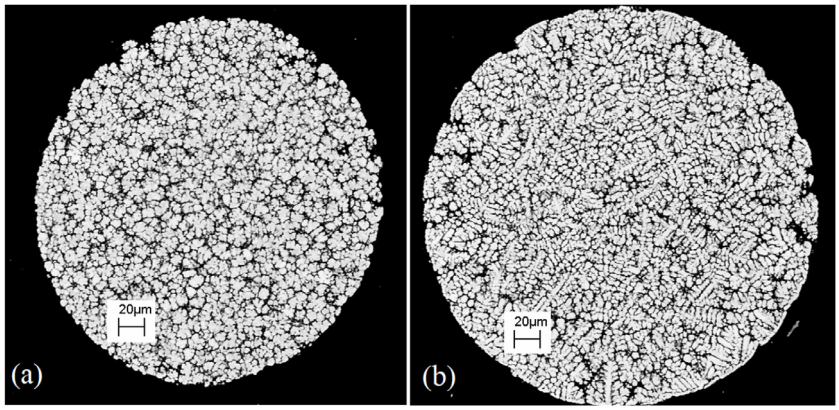

Fig. 9. Scanning electron microscope (SEM) image of Al-40at.% Ni samples solidified under reduced gravity in EML established within the TEXUS sounding rocket. (a) Droplet solidified at the undercooling $\Delta T = 123$K which is consistent with the downward part of the velocity curve, $dV/d(\Delta T) < 0$, shown in Fig. 2(c). (b) Droplet solidified at the undercooling $\Delta T = 275$K which is consistent with the upward part of the velocity curve, $dV/d(\Delta T) > 0$, shown in Fig. 2(c).

the experimentally measured front velocity has the form of the downward curve or upward curve. Figure 9 demonstrates two different microstructures of Ni-40at.%Al droplets processed in EML under reduced gravity conditions. The difference in dendritic structure is clearly visible. The droplet solidified at $\Delta T =$ 123K exhibits small equiaxed dendrites appearing after multiple crystals nucleation, see Fig. 9(a). The high-speed camera fixed stripes/waves at the solidification front (front of recalescence) on the surface of this droplet. Quantitatively, the solidification rate of this droplet is related to the downward part of the velocity curve, $dV/d(\Delta T) < 0$, shown in Fig. 2(c). By contrast, the structure of the droplet solidified at $\Delta T = 275$K is visible as disordered dendrites with long stems and developed secondary branches, see Fig. 9(b). Solidification of this droplet exhibited propagation of the rugged/flat front of recalescence recorded by the high-speed camera that was quantitatively consistent with the upward part of the velocity curve, $dV/d(\Delta T) > 0$, shown in Fig. 2(c).

The results presented in Figs. 7, 8, and 9 are in full agreement with the obtaining of recent studies [32,33]. They also directly indicate that it is necessary to consider not only the growth process, but another process competing with growth to predict descending solidification rate curves. This additional process is the nucleation of crystals, which is confirmed by our theoretical calculations in next Section exhibiting the appearance of downward velocity curves with increasing undercooling.

4. Theoretical modeling

Since it has been experimentally established that the kinetics of solidification is determined by the nucleation and growth of crystals, a theoretical description should include these two processes. The model [33] considers the motion of a two-phase zone precisely due to the successive nucleation of crystals that is schematically shown in Fig. 10(a). Namely, this figure illustrates that the boundary “Solid phase – Two-phase zone” moves due to predominant nucleation of newly born crystals with their attachment to the so-called “Solid crystalline front”. Therefore, in the first case, the boundary “Two-phase zone – liquid phase” moves by after the nucleation giving the velocity $|V_{nucl}|$. Competition between nucleation and growth may drive the boundaries of the two-phase zone and the solidification kinetics is defined by the preferable process. Another limiting case is considered as a predominant directional growth. In this case, the solidification velocity is V_{front}, shown in Fig. 10(b). As a result, the recalescence front moves with the velocity $V_{rec} = |V_{nucl}| + V_{front}$. The predominance of growth or nucleation must be selected kinetically, which we will show in the extended version of the model which includes growth and nucleation of crystals simultaneously.

Equations from our previous work [33] were transformed according to the treatments of the original works [34–36]. Now, after transformations of the model equations, they are presented in the form of dimensional functions and parameters.

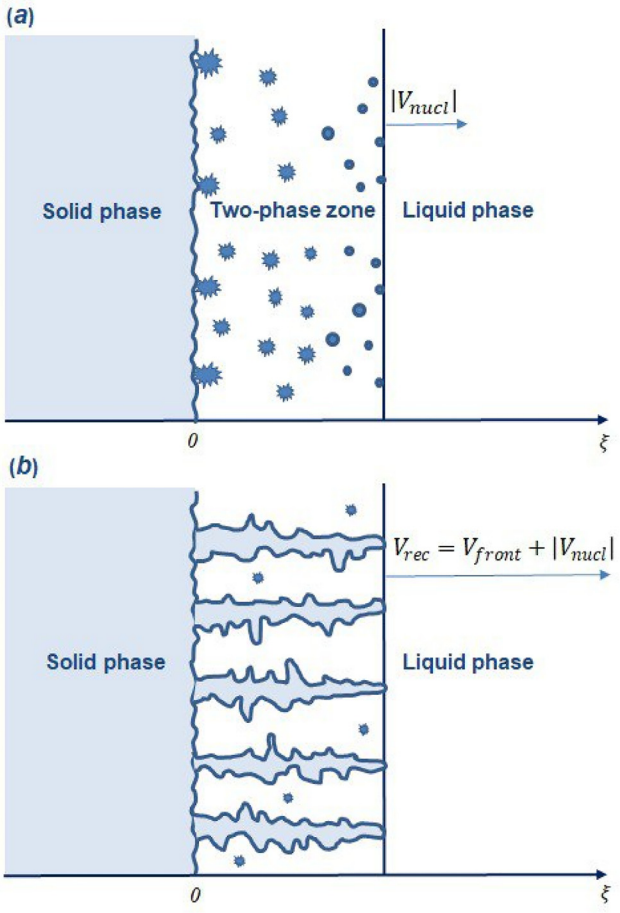

Fig. 10. Illustration of the moving two-phase zone along the spatial coordinate ξ at time τ. The velocity $V_{nucl}(\tau)$ due to crystal nucleation is driving by the undercooling $\Delta T_{nucl}(\tau)$. The velocity $V_{front}(\tau)$ due to crystal growth is driving by the undercooling $\Delta T_{front}(\tau)$. Panel (a) shows a solidification regime with predominant nucleation while panel (b) illustrates both contributions from nucleation and directional growth resulting in the recalescence velocity $V_{rec} = |V_{nucl}| + V_{front}$.

The undercooling balance ΔT is defined as a sum of nucleation undercooling $\Delta T_{nucl}(\tau)$ and the undercooling at the boundary "Solid phase – Two-phase zone" denoted by $\Delta T_{front}(\tau)$ (see Fig. 10):

$$\Delta T(\tau) = \Delta T_{nucl}(\tau) + \Delta T_{front}(\tau), \tag{1}$$

$$\Delta T_{nucl}(\tau) = \Delta T_0\left[F_0(\xi,\tau) + \epsilon I_0^{k/4}\beta_*^{3k/4}\Delta T_0^{3k/4}\tau^k F_1(\xi,\tau)\right], \tag{2}$$

$$\Delta T_{front}(\tau) = \left(\frac{V_{front}}{\mu_k}\right)^{1/n}, \tag{3}$$

where ΔT_0 represents initial undercooling, ξ is dimensional spatial coordinate, τ is dimensional time, I_0 is initial nucleation rate (frequency), β_* is a kinetic parameter, k is a constant for kinetic regime, μ_k is a kinetic coefficient, and n is a power parameter that can be found numerically. Parameter ϵ can be designated as

$$\epsilon = \alpha_* A,$$

where

$$\alpha_* = \frac{\beta_* L_V}{\lambda_l}\left(\frac{\beta_*\Delta T_0}{I_0}\right)^{1/4}, \quad A = \frac{3b^{3/4}\Gamma(1/4)}{b_0\alpha_*^2 p^{1/4}}, \quad b = \frac{4\pi L_V}{3\rho c\Delta T_0}.$$

Here L_V is latent heat of crystallization, λ_l is a thermal conductivity of the liquid phase, Γ is a Gamma function, b_0 is a constant in the case of the Weber-Volmer-Frenkel-Zel'dovich (WVFZ) kinetics (see [37–42]), ρ is a density of the liquid phase, and c_p is the thermal capacity of the liquid phase.

Parameter p defining the nucleation rate (frequency) is an exponential function of the energy barrier height and in the case of the WVFZ kinetics has the form of the dimensionless Gibbs number (see, for details, [52])

$$p = \frac{16\pi\gamma_i^3 T_p}{3L_V^2\Delta T_0^2 k_B}, \tag{4}$$

where γ_i is the surface tension and k_B is the Boltzmann constant.

The interface velocity $V(\tau)$ due to nucleation and growth of crystals, Fig. 10, is given by

$$V(\tau) = V_{rec} = V_{nucl}(\tau) + V_{front}(\tau), \tag{5}$$

$$V_{nucl}(\tau) = \left(\frac{\beta_*\Delta T_0}{I_0}\right)^{1/4}\left[\frac{\alpha I_0^{1/8}\beta_*^{3/8}\Delta T_0^{3/8}}{2\sqrt{\tau}} + \epsilon\beta\frac{7}{2}\tau^{5/2}I_0^{7/8}\beta_*^{21/8}\Delta T_0^{21/8}\right], \tag{6}$$

$$V_{front}(\tau) = \mu_k\Delta T^n. \tag{7}$$

Constants α and β from Eq. (6) should be found from equations

$$\mathrm{erfc}\left(\frac{\alpha}{2\sqrt{\gamma}}\right) + w_\infty\mathrm{erf}\left(\frac{\alpha}{2\sqrt{\gamma}}\right) = 0, \tag{8}$$

$$\beta = \sqrt{\pi\gamma}\,\mathrm{erf}\left(\frac{\alpha}{2\sqrt{\gamma}}\right)\exp\left(\frac{\alpha^2}{4\gamma}\right)F_1(\alpha), \tag{9}$$

where

$$w_\infty = \frac{T_p - T_\infty}{\Delta T_0}, \quad \gamma = \frac{\lambda_l I_0^{1/4}}{\rho c\beta_*^{5/4}\Delta T_0^{5/4}}.$$

Functions F_0 and F_1 from Eq. (2) are given by

$$F_0(\xi,\tau) = 1 - \frac{\mathrm{erf}\left(\frac{I_0^{1/8}}{\beta_*^{5/8}\Delta T_0^{5/8}}\frac{\xi}{\sqrt{\tau}}\frac{1}{2\sqrt{\gamma}}\right)}{\mathrm{erf}\left(\frac{\alpha}{2\sqrt{\gamma}}\right)}, \tag{10}$$

$$F_1(\xi,\tau) = \int_0^{\frac{I_0^{1/8}\xi}{\beta_*^{5/8}\Delta T_0^{5/8}\sqrt{\tau}}}[\Omega(\xi_1) - \Omega(\alpha)]\exp\left(-\frac{\xi_1^2}{4\gamma}\right)d\xi_1, \tag{11}$$

where

$$\Omega(\xi_1) = \frac{1}{\gamma}\int_0^{\xi_1}\Psi(\xi_2)\exp\left(\frac{\xi_2^2}{4\gamma}\right)d\xi_2,$$

$$\Psi(\xi_2) = 4K^2(\xi_2)\xi_2^4 F_0(\xi_2), \quad K(\xi_2) = \int_{\xi_2}^{\infty}\frac{F_0(\xi_3)}{\xi_3^3}d\xi_3.$$

In these expressions, $F_0(\xi_3)$ should be substituted as

$$F_0(\xi_3) = 1 - \frac{\mathrm{erf}\left(\frac{\xi_3}{2\sqrt{\gamma}}\right)}{\mathrm{erf}\left(\frac{\alpha}{2\sqrt{\gamma}}\right)}.$$

To compare the theoretical prediction and the experimental data, one fundamental difference should be noted between the data obtained by such methods. Solution of Eqs. (1)-(11) predicts how velocity $V(\tau)$ and undercooling $\Delta T(\tau)$ change with time τ and along the distinguished spatial direction ξ. Figure 2, on the contrary, shows the dependence of the initial, starting undercooling ΔT_0 on the velocity V, averaged over the diameter of the near-spherical sample. Moreover, in many experiments, it was shown that the velocity of the crystal front or the velocity of the dendrites quickly reaches its constant value and the process is considered quasi-stationary. Experimentally, this was shown, for

Table 1
Material parameters of Al-Ni alloy used in calculations.

Parameter	Value	Units	Source
Phase transition temperature, T_p	1673	K	[43]
far from the crystallization front, T_∞	1900	K	[43]
Latent heat of crystallization, L_V	567	kJ·kg·m^{-3}	[43]
Thermal conductivity of a liquid phase, λ_l	86.2	J·m^{-1}·s^{-1}·K^{-1}	[43]
Thermal capacity of the liquid phase, c	1040	J·kg^{-1}·K^{-1}	[43]
Kinetic parameter, β_*	10^{-3}	m·s^{-1}·K^{-1}	present work
Initial nucleation rate, I_0	10^{20}	m^{-3}·s^{-1}	present work
Density of liquid phase, ρ	4290	kg·m^{-3}	present work
Kinetic coefficient, μ_k	$2{\cdot}10^{-3}$	m·s^{-1}·K^{-1}	present work
Surface tension, γ_i	0.115	J·m^{-2}	present work

Table 2
Parameters of Al-Ni alloy used in calculations by Eqs. (1)–(11).

Parameter	Value	Units	Source
b_0	$2^{7/4}$	-	[34]
k	3	-	[34]
n	3	-	present work
p	$8.2{\cdot}10^2$	-	present work
α_*	3.4	-	present work
A	0.3	-	present work
b	10.3	-	present work
ϵ	1.1	-	present work
γ	0.72	-	present work

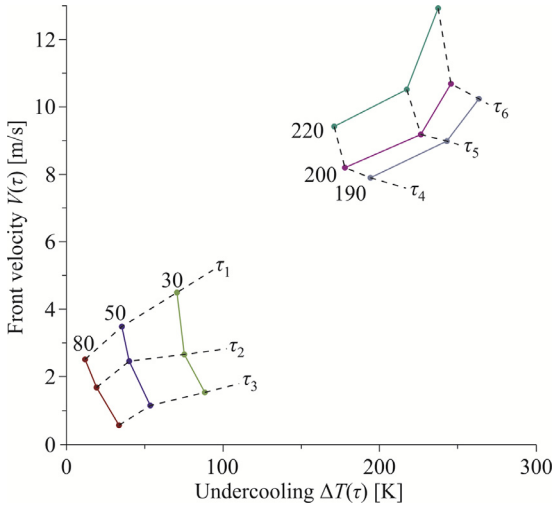

Fig. 11. Calculated front velocity $V(\tau)$ versus undercooling $\Delta T(\tau)$ of the Al-Ni alloy at different times $\tau_1 < \tau_2 < ... < \tau_6$. The points represent the average velocity $V(\tau)$ on the distance $\xi = 10^{-3}$ (m). The numbers at the curves indicate the starting (nucleation) undercooling ΔT_0. Solid lines indicate change of $V(\tau)$ with $\Delta T(\tau)$ at a given initial ΔT_0. Dashed lines show isochores by which velocity changes with ΔT_0 to connect such tendency with experimental data shown in Fig. 2.

instance, in [1,2,47,49,51] and, theoretically, such quick approach from non-stationary mode to steady state solidification in undercooled droplets has been proved in [53]. The velocity in Ni-Al samples shown in Fig. 2 was not estimated in detail of its reaching the quasi-stationary regime. Therefore, model predictions using the equations (1)-(11) can be compared with experiment if it is possible to estimate how the velocity $V(\tau)$ changes with increasing initial undercooling ΔT_0 in the region of relatively small values of non-stationary undercooling $\Delta T(\tau)$ and in the region of relatively large values of non-stationary undercooling $\Delta T(\tau)$.

The system of Eqs. (1)-(11) has been solved numerically using the materials and numeric parameters of Tables 1 and 2. Initial undercooling, ΔT_0, has been varied in calculations as: 30K, 50K, 80K 190K, 200K, and 220K. The temporal change of the velocity has been estimated at the distance $\xi = 10^{-3}$m from the outer surface of the near-spherical droplet which usually has the diameter of $\xi = (6...7) \cdot 10^{-3}$m as a sample processed in electromagnetic levitator [1,2].

Figure 11 represents the obtained analytical solution in the case of the kinetic growth mode [34]. It is seen that with the increasing time ($\tau_1 < \tau_2 < \tau_3$) and in the range of the smallest undercooling, $\Delta T < 100$K, the front velocity decreases. This occurs due to the predominant contribution of nucleation of crystals into the motion of the observed solidification front shown in the scheme of Fig. 10(a). Such behavior is consistent with experimental data for Al-25at.% Ni, Al-31.5at.% Ni, and Al-40at.% Ni alloys shown in Fig. 2 at smallest values of undercooling.

From Fig. 11 it is also seen that with the increasing time ($\tau_4 < \tau_5 < \tau_6$) and in the range of the largest undercooling, $\Delta T > 180$K,

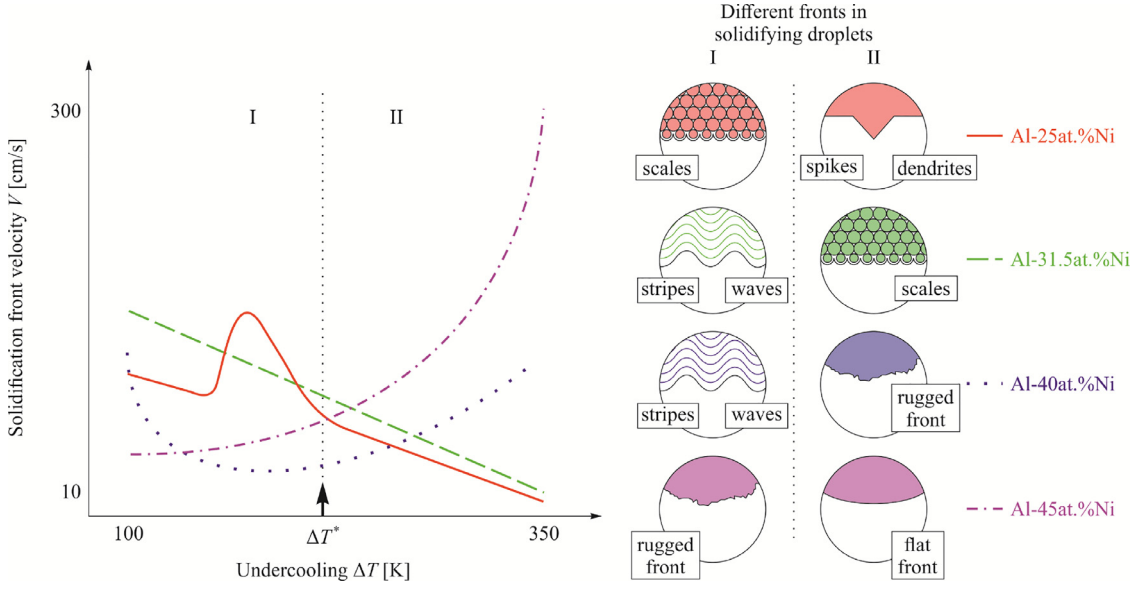

Fig. 12. Classification of solidification morphologies observed on the surfaces of Al-Ni droplets processed in EML on the Ground, under reduced gravity (in parabolic flights), and in microgravity (onboard the ISS). Classification is given by the behavior of solidification front velocity V as function of undercooling ΔT. Range *I* shows patterns below critical undercooling, i.e. for $\Delta T < \Delta T^*$. Range *II* shows patterns above critical undercooling, i.e. for $\Delta T > \Delta T^*$.

the front velocity increases. This occurs due to the predominant contribution of crystal growth into the motion of the observed solidification front shown in the scheme of Fig. 10(b). Such behavior is consistent with experimental data for Al-40at.% Ni for the largest values of undercooling $\Delta T > 175$K or for Al-45at.% Ni alloy in the whole range of ΔT shown in Fig. 2.

Thus, the solution of Eqs. (1)-(11), which includes the propagation of the solidification front due to the nucleation or growth of crystals, confirms the experimental results shown in Fig. 2. The data showing the decreasing velocity with increasing undercooling are due to the predominant nucleation of crystals. The data on the velocity, which increases with increasing undercooling, are due to the movement of the solidification front provided by the crystalline growth.

5. Conclusions

Solidification kinetics of four different Al-Ni alloy samples, particularly, of Al-25at.% Ni, Al-31.5at.% Ni, Al-40at.% Ni and Al-45at.% Ni alloys, processed in the Electromagnetic Levitation Facility (EML) on the Ground, under reduced gravity (in parabolic flights and TEXUS sounding rockets) and in microgravity (in ISS - International Space Station) are critically analyzed. Analysis has been done in comparison with the previous results of Lengsdorf et al. on solidification kinetics [29], data on crystal nucleation and metallographic findings presented in recent works [8,32].

Analysis of high-speed-camera digital videos allows us to classify recalescence patterns at the surface of solidifying samples in EML as scales, spikes (or dendrites with sharp tips), stripes (or wavy fronts), rough front, and flat (planar) front. These patterns reproduce crystalline morphology changing as the undercooling and chemical composition change. Measured front velocities for these patterns are summarized in Fig. 2 by previously and newly obtained data on solidification kinetics of Al-rich Al-Ni alloys. Each of the kinetic curves "front velocity V - undercooling ΔT" can be conditionally divided by the critical undercooling $\Delta T = \Delta T^*$ into two parts. Every part of the curve for each of the Al-Ni alloys is characterized by its own recalescence pattern, i.e. by the particular crystal morphology in solidifying samples. This is clearly shown in the diagram of Fig. 12.

Characterizing the solidification behavior by recalescence patterns at the surface of solidifying samples and by final microstructure in metallographic analysis, we prove that instead of "growth front morphology" the high-speed videos reproduce the complicated simultaneous processes of crystal nucleation and their growth. These coupled processes are visible as the scales, spikes (or dendrites with sharp tips), and stripes (wavy fronts) at small and intermediate values of undercooling in solidifying Al-25at.% Ni, Al-31.5at.% Ni, and Al-40at.% Ni alloys at $\Delta T < \Delta T^*$ in Fig. 12. Moreover, in these alloys and at these undercoolings the solidification kinetics is given by the negative slope of the velocity V - undercooling ΔT relationship, i.e. at $dV/d(\Delta T) < 0$. Such anomalous behavior is forbidden by the crystal growth theory [27,30] proving existence of the stable "front velocity V - undercooling ΔT" relationship only with its positive slope, $dV/d(\Delta T) > 0$. By contrast, intermediate and higher values of undercooling at $\Delta T > \Delta T^*$ provide a preferable crystal growth with the positive slope, $dV/d(\Delta T) > 0$, in Al-40at.% Ni alloy and in the whole range of measured undercooling in the Al-45at.% Ni alloy, see Fig. 12.

The multiple nucleation events together with the crystal growth may lead to the kinetic curves with $dV/d(\Delta T) < 0$ that is proved by recalescence patterns and metallography analysis of the present work together with the sequence of proves presented by Eqs. (1)-(11). As the experimental metallography analysis, the negative slope of the "front velocity V - undercooling ΔT" curve is suggested to be a consequence of multiple nucleation events in the vicinity of previously formed nuclei that is proved by theoretical calculations based on the equations given in Section 4. The calculated velocity depends on the time due to the non-stationarity of the crystal nucleation process. The experimentally measured value of velocity is defined by the quasi-stationary process of solidification of the droplet. However, these two processes have been combined with interpreting of the downward and upward branches of the experimental velocity. The mathematical model (Section 4) shows that there is a predominance of crystal nucleation, which slows down the movement of the crystallization front with increasing undercooling. However, in this model, there is a critical point (extremum point), beyond which crystal growth begins to dominate over nucleation, and the crystallization front velocity begins to increase with increasing undercooling. Indeed, based on a theoretical model (Section 4), Fig. 11 shows isochores for several selected undercoolings. It is shown that the velocity decreases and the undercooling increases for times $\tau_1 < \tau_2 < \tau_3$ (for every given initial undercooling compatible with the undercooling in Fig. 2). This behavior gives a downwards velocity branch, $dV/d(\Delta T) < 0$, at relatively low initial values of undercooling. In contrast, the velocity increases with increasing undercooling for times $\tau_4 < \tau_5 < \tau_6$ (for every given initial undercooling consistent with the undercooling in Fig. 2). This behavior gives an upwards velocity branch, $dV/d(\Delta T) > 0$, at relatively large initial values of undercooling. Thus, Fig. 2 (experimental data on the solidification velocity of undercooled droplets) becomes qualitatively explicable from the standpoint of the analysis of Fig. 11 (theoretically calculated crystallization velocity).

As a prospective development of this work, one can interpret the nucleation front velocity in Al-rich Al-Ni alloys which solidify with the negative temperature gradient ahead of the solid-liquid interface. In particular, computational modeling may clarify why the nucleation does not develop ahead of the solid-liquid front (i.e. in bulk liquid) despite a larger driving force. It should be additionally noted that even the mesoscopic mechanism of changes of the velocity curves from 31.5-at%Ni to 40at%Ni is not completely clarified so far. In this case, we observed that only several Ni percents lead to the change of the velocity curve from its completely downward slope (Fig. 2(b) where $dV/d(\Delta T) < 0$) to the upward slope (Fig. 2(c) where $dV/d(\Delta T) < 0$ changes to $dV/d(\Delta T) > 0$). Indeed, as is discussed and analyzed in [54,55], multiphase solidification behavior given by the formation of peritectic structure, eutectics, and intermetallics can be rather complex in the aluminum-rich region of the Al-Ni alloy especially dependent on the total undercooling prior to nucleation and growth of leading crystal pattern. In this context, the competition between volumetric undercooling for nucleation and crystal-liquid interface undercooling for growth plays a crucial role in the change of the velocity curve slopes. Particularly, the change of overall crystal-liquid interface undercooling, which depends on the change of several kinetic processes such as disorder trapping, solute drag, and its redistribution with non-equilibrium trapping would be expected with changing the nominal alloy's composition [55]. Therefore, detailed computations of the undercooling contributions for various compositions and their role in nucleation-growth processes are seen as the further development of the current work.

Declaration of Competing Interest

We declare that the present manuscript present principally novel results on crystallization kinetics of Al-Ni alloys. The presently chosen Al-rich Al-Ni alloys exhibit unusual behavior by decreasing the crystallization velocity with the increase of undercooling. Such behavior contradicts the usual understanding, coming from the thermodynamics of irreversible processes, according to which the reaction of the system (crystallization velocity) should

increase with the increase of driving force on transformation (undercooling). However, we present clear proof that crystallization kinetics is mainly defined not by the growth but by the nucleation of crystals ahead of the solidification front. The developed theoretical model confirms the existence of the decreasing of the crystallization velocity with the increase of undercooling.

We believe that the experimental results (obtained in microgravity, namely, on board of International Space Station, and on the Ground) are of great interest to many researchers in materials sciences. Therefore, we hope that the present manuscript is adjusted to the requirements of the journal "ACTA MATERIALIA" and believe that the manuscript can be considered for publication.

Declaration of Competing Interest

The authors declare that they have no known competing financial interests or personal relationships that could have appeared to influence the work reported in this paper.

Acknowledgements

The present work is dedicated to the blessed memory of Professor Dieter Matthias Herlach who made a study of rapid solidification qualitatively clear and quantitatively accessible. The financial support by the European Space Agency (ESA) within the project NEQUISOL under contract No. 15236/02/NL/SH for experimental measurements under reduced gravity and by RSF under project No. 21-19-00279 for theoretical modeling is acknowledged. P.K.G. acknowledges the support from the German Space Center - Space Administration under contract No. 50WM1941 and Y.F. acknowledges the support of the German Science Foundation (DFG) under the Project GA 1142/11-1 for experimental measurements on the Ground. The authors specially thank ESA and its representative Dr. Wim Sillekens for the opportunity to use the ISS-EML and the team from Microgravity User Support Center (MUSC) at Deutsches Zentrum für Luft- und Raumfahrt (DLR-Köln) for the support with the Electromagnetic Levitator onboard the International Space Station (ISS-EML). Valuable discussions with Matthias Kolbe and Andrew Mullis on solidification behaviour of Al-Ni alloys are acknowledged. The experiments on Al-reach Al-Ni alloys and, especially, on Al-25% Ni were carried out in cooperation with the Institut für Materialphysik im Weltraum at the DLR-Köln. For support with the carrying out EML experiments in DLR-Köln we thank Stefan Burggraf and Stefanie Koch. Authors specially thanks Johannes Wilke, Hans-Jürgen Hempel and Jürgen Brozek for the support with in-house equipment by FSU-Jena.

References

[1] D.M. Herlach, D.M. Matson, Solidification of Containerless Undercooled Melts, Wiley, Weinheim, 2012.
[2] D.M. Herlach, P.K. Galenko, D. Holland-Moritz, Metastable Solids from Undercooled Melts, Elsevier, Amsterdam, 2007.
[3] H. Assadi, M. Barth, A.L. Greer, D.M. Herlach, Kinetics of solidification of intermetallic compounds in the NI-AL system, Acta Mater. 46 (2) (1998) 491–500.
[4] H. Assadi, S. Reutzel, D.M. Herlach, Kinetics of solidification of B2 intermetallic phase in the Ni-Al system, Acta Mater. 54 (10) (2006) 2793–2800.
[5] H. Assadi, M. Oghabi, D.M. Herlach, Influence of ordering kinetics on dendritic growth morphology, Acta Mater. 57 (5) (2009) 1639–1647.
[6] D.M. Herlach, R. Lengsdorf, P.K. Galenko, H. Hartmann, C.-A. Gandin, S. Mosbah, A. Garcia-Escorial, H. Henein, Non-equilibrium and near-equilibrium solidification of undercooled melts, Adv. Eng. Mater. 10 (5) (2008) 444–452.
[7] D.M. Herlach, S. Binder, P.K. Galenko, J. Gegner, D. Holland-Moritz, S. Klein, M. Kolbe, T. Volkmann, Containerless undercooled melts: Ordering, nucleation, and dendrite growth, Metall. Mat. Trans. A 46 (2015) 4921–4936.
[8] D.M. Herlach, S. Burggraf, P.K. Galenko, C.-A. Gandin, A. Garsia-Escorial, H. Henain, C. Karrasch, A. Mullis, M. Rettenmayr, J. Valloton, Solidification of undercooled melts of Al-based alloys on earth and in space, JOM 69 (8) (2017) 1303–1310.
[9] S. Reutzel, H. Hartmann, P.K. Galenko, S. Schneider, D.M. Herlach, Change of the kinetics of solidification and microstructure formation induced by convection in the nial system, Appl. Phys. Lett. 91 (2007). 0419113-1-3
[10] W. Löser, O. Shuleshova, H.-G. Lindenkreuz, B. Büchner, Melt undercooling experiments for raney-Ni type Ni-50wt.% Al alloys, in: H. Jones (Ed.), Solidification processing, University of Sheffield, Sheffield, 2007.
[11] O. Shuleshova, Equilibrium and metastable solidification in Ti-Al-Nb and Al-Ni systems, Dissertation, Technische Universität Dresden, Dresden, 2009.
[12] O. Shuleshova, D. Holland-Moritz, W. Löser, G. Reinhart, G.N. Iles, B. Büchner, Metastable formation of decagonal quasicrystals during solidification of undercooled al-ni melts: In situ observations by synchrotron radiation, EPL 86 (3) (2009). 36002-1-4
[13] O. Shuleshova, D. Holland-Moritz, W. Löser, H.-G. Lindenkreuz, B. Büchner, In situ observation of phase selection in undercooled ni-al melts, Int. J. Cast Met. Res. 22 (1-4) (2013) 286–289.
[14] A.L. Greer, H. Assadi, Rapid solidification of intermetallic compounds, Mater. Sci. Eng. A 226-228 (1997) 133–141.
[15] A. Kerrache, J. Horbach, K. Binder, Molecular-dynamics computer simulation of crystal growth and melting in $al_{50}ni_{50}$, EPL 81 (2008). 58001-1-4
[16] X.O. Zhang, Y. Yang, Y.F. Gao, J.J. Hoyt, M. Asta, D.J. Sun, Disorder trapping during crystallization of the b2-ordered nial compound, Phys. Rev. B 85 (2012). 041601-1-7
[17] H. Assadi, A phase-field model for non-equilibrium solidification of intermetallics, Acta Mater. 55 (2007) 5225–5235.
[18] P.K. Galenko, A. Salhoumi, V. Ankudinov, Kinetics of rapid crystal growth: phase field theory versus atomistic simulations, IOP Conf. Series: Mat. Sci. Eng. 529 (2019). 012035-1-5
[19] H. Hartmann, D. Holland-Moritz, P.K. Galenko, D.M. Herlach, Evidence of the transition from ordered to disordered growth during rapid solidification of an intermetallic phase, EPL 87 (2009). 40007-1-4
[20] W.J. Boettinger, M.J. Aziz, Theory for the trapping of disorder and solute in intermetallic phases by rapid solidification, Acta Metall. 37 (1989) 3379–3391.
[21] A.A. Chernov, Kinetic phase transitions, Sov. Phys. JETP 26 (1968) 1182–1190.
[22] A.A. Chernov, Growth of copolymer chains and mixed crystals – trial and error statistics, Sov. Fis. Usp. 13 (1970) 101–128.
[23] D.E. Temkin, Kinetic phase transition during a phase conversion in a binary alloy, Sov. Phys. Cryst. 15 (1971) 773–780.
[24] E.A. Brener, D.E. Temkin, Kinetics of normal growth of ordering crystal, Sov. Phys. Cryst. 28 (1983) 7–16.
[25] E.A. Brener, D.E. Temkin, Kinetic transition during the growth of a crystal under ordering, Sov. Phys. Cryst. 28 (1983) 142–149.
[26] P.K. Galenko, I.G. Nizovtseva, K. Reuther, M. Rettenmayr, Kinetic transition in the order–disorder transformation at a solid/liquid interface, Philos. Trans. R. Soc. A 376 (2018). 20170207-1-12
[27] P.K. Galenko, D. Jou, Rapid solidification as non-ergodic phenomenon, Phys. Rep. 818 (2019) 1–70.
[28] R. Lengsdorf, P.K. Galenko, D.M. Herlach, Measurement of dendrite growth on AL-NI alloys in reduced gravity, in: H. Lacoste (Ed.), European rocket and balloon programmes and related research, European Space Agency Communication Production Office, Noordwijk, 2009.
[29] R. Lengsdorf, D. Holland-Moritz, D.M. Herlach, Anomalous dendrite growth in undercooled melts of alni alloys in relation to results obtained in reduced gravity, Scr. Mater. 62 (2010) 365–367.
[30] P.K. Galenko, D.A. Danilov, Selection of the dynamically stable regime of rapid solidification front motion in an isothermal binary alloy, J. Cryst. Growth 216 (2000) 512–526.
[31] K. Reuther, P.K. Galenko, M. Rettenmayr, Dynamic instability of the steady state of a planar front during nonequilibrium solidification of binary alloys, J. Cryst. Growth 506 (2019) 55–60.
[32] D.M. Herlach, S. Burggraf, M. Reinartz, P.K. Galenko, M. Rettenmayr, C.-A. Gandin, H. Henein, A. Mullis, A. Ilbagi, J. Valloton, Dendrite growth in undercooled al-rich al-ni melts measured on earth and in space, Phys. Rev. Mater. 3 (2019). 073402-1-7
[33] M. Reinartz, M. Kolbe, D.M. Herlach, M. Rettenmayr, L.V. Toropova, D.V. Alexandrov, P.K. Galenko, Study on anomalous rapid solidification of Al-35at.% Ni alloy in microgravity, JOM 74 (2022) 2420–2427.
[34] D.V. Alexandrov, Dynamics of the phase transition boundary in the presence of nucleation and growth of crystals, J. Phys. A: Math. Theor. 50 (2017). 345101-1-11
[35] D.V. Alexandrov, A.A. Ivanov, I.V. Alexandrova, Analytical solutions of mushy layer equations describing directional solidification in the presence of nucleation, Philos. Trans. R. Soc. A 376 (2018) 20170217.
[36] L.V. Toropova, D.V. Alexandrov, Dynamical law of the phase interface motion in the presence of crystals nucleation, Scientific Reports 12 (2022) 10997.
[37] M. Volmer, A. Weber, Keimbildung in übersättigten gebilden, Z. Phys. Chem. 119 (1926) 277–301.
[38] M. Volmer, Kinetik der Hasenbildung, Steinkopf, Dresden, Germany, 1939.
[39] R. Becker, W. Döring, Kinetische behandlung der keimbildung in übersättigten dämpfern, Ann. Phys. 24 (1935) 719–752.
[40] J. Frenkel, Kinetic theory of liquids, Dover, New York, NY, 1955.
[41] J.B. Zel'dovich, On the theory of formation of new phases: cavitation, J. Exp. Theor. Phys. 12 (1942) 525–538.
[42] E.M. Lifshitz, L.P. Pitaevskii, Physical kinetics, Pergamon, Oxford, UK, 1981.
[43] D. Holland-Moritz, I. Egry, T. Matsushita, S. Seetharaman, R. Brooks, R. Wunderlich, IMPRESS project deliverable d7.6, thermophysical properties database (for Al-Ni alloys), NMP3-CT-2004500635, 2008.

[44] C.W. Bale, E. Belisle, P. Chartrand, S.A. Decterov, G. Eriksson, A.E. Gheribi, K. Hack, I.-H. Jung, Y.-B. Kang, J. Melancon, A.D. Pelton, S. Petersen, C. Robelin, J. Sangster, P. Spencer, M.A. van Ende, Factsage thermochemical software and databases 2010-2016, Calphad 54 (2016) 35–53.
[45] D. Grushko, T.Y. Velikanova, Formation of quasicrystals and related structures in systems of aluminum with transition metals. part 1. binary systems formed by aluminum with 3d metals, Powder Metall. Met. Ceram. 43 (1/2) (2004) 72–86.
[46] G.J. Ehlen, D.M. Herlach, Investigation of solidification in undercooled al-rich al-ni alloy systems, IOP Conf. Ser.: Mater. Sci. Eng. 33 (2012). 012066-1-4
[47] M. Reinartz, Study on the Growth Anomaly in Al-Ni Melts under Gravity and Microgravity Conditions, Friedrich-Schiller-Universität, Jena, 2020 Phd dissertation.
[48] A.M. Mullis, A model for the anomalous velocityundercooling behaviour of levitated AL-NI alloys onboard the international space station, Microgravity Sci. Technol. 33 (2021). 70-1-20
[49] P.K. Galenko, R. Hanke, P. Paul, S. Koch, M. Rettenmayr, J. Gegner, D.M. Herlach, W. Dreier, E.V. Kharanzhevski, Solidification kinetics of CuZr alloy: Ground-based and microgravity experiments, IOP Conf. Series: Mater. Sci. Eng. 192 (2017). 012028-1-11
[50] D.M. Matson, S.P. Marsh, J.A. Dantzig, R. Trivedi, W. Hofmeister, M.G. Chu, E.J. Lavernia, The measurement of dendrite tip propagation velocity during growth into undercooled metallic melts, in: J.H. Chun (Ed.), Solidification 1998, TMS, Warrendale, PA, 1998, p. 233.
[51] O. Funke, G. Phanikumar, P.K. Galenko, L. Chernova, S. Reutzel, M. Kolbe, D.M. Herlach, Dendrite growth velocity in levitated undercooled nickel melts, J. Cryst. Growth 297 (2006) 211–222.
[52] D.V. Alexandrov, A.P. Malygin, Transient nucleation kinetics of crystal growth at the intermediate stage of bulk phase transitions, J. Phys. A: Math. Theor. 46 (2013) 455101.
[53] E.A. Titova, P.K. Galenko, D.V. Alexandrov, Method of evaluation for the non-stationary period of primary dendritic crystallization, J. Phys. Chem. Solids 134 (2019) 176–181.
[54] H. Assadi, A.L. Greer, Site-ordering effects on element partitioning during rapid solidification of alloys, Nature 383 (1996) 150–152.
[55] H. Assadi, A.L. Greer, The interfacial undercooling in solidification, J. Cryst. Growth 172 (1997) 249–258.